2D Materials

PAPER

Trap induced long exciton intervalley scattering and population lifetime in monolayer WSe_2

2D Materials

PAPER

RECEIVED
24 November 2020

REVISED
8 March 2021

ACCEPTED FOR PUBLICATION
8 April 2021

PUBLISHED
26 April 2021

Trap induced long exciton intervalley scattering and population lifetime in monolayer WSe_2

Julian Wagner, Henning Kuhn, Robin Bernhardt, Jingyi Zhu* and Paul H M van Loosdrecht*

Universität zu Köln, II. Physikalisches Institut, D-50937 Köln, Germany
* Authors to whom any correspondence should be addressed.

E-mail: jzhu@ph2.uni-koeln.de **and** pvl@ph2.uni-koeln.de

Keywords: transient grating, heterodyne detection, intervalley scattering, monolayer WSe_2, valley polarization, exciton population lifetime, exciton phonon scattering

Supplementary material for this article is available online

Abstract

Monolayer transition metal dichalcogenides (TMDCs) hold the best promise for next generation optoelectronic and valleytronic devices. However, their actual performance is usually largely affected by the presence of inevitable defects. Therefore, a detailed understanding of the influence of defects on the dynamic properties is crucial for optimizing near future implementations. Here, the exciton population and valley scattering dynamics in a chemical vapor deposition grown large size monolayer WSe_2 with naturally abundant vacancy and boundary defects were systematically investigated using polarization controlled heterodyned transient grating spectroscopy at different excitation wavelengths and temperatures. Slow and multi-exponential decay dynamics of the exciton population were observed while no sign of any micron scale diffusive transport was identified, consistent with the effect of exciton trapping by defects. In general, two different kinds of exciton species were identified: one with short population lifetime (∼10 ps) and extremely fast intervalley scattering dynamics (<200 fs) and in contrast another one with a long population lifetime (>1 ns) and very slow intervalley scattering dynamics exceeding 100 ps. We assign the former to non-trapped excitons in the nanometer scale and the latter to defect-bound excitons. Temperature dependent intervalley scattering dynamics of the trapped excitons can be understood in terms of a two optical phonon dominated process at the *K* point in momentum space. Our findings highlight the importance of the intrinsic defects in monolayer TMDCs for manipulating exciton valley polarization and population lifetimes, which is key for future device applications.

1. Introduction

The interplay of dimensionality and existence of symmetries in solid materials leads to interesting physical phenomena and fascinating properties. In two-dimensional (2D) monolayer transition metal dichalcogenides (TMDCs) the interplay between the breaking of spatial inversion symmetry and the strong spin-orbit coupling results in a novel quantum mechanical degree of freedom, the valley pseudospin, which can be experimentally addressed by circularly polarized light [1, 2]. These unique characters of the monolayer TMDCs offer a highly attractive platform for future valleytronic devices and provide a fruitful testbed for valley information storage [3].

At the current stage, many time-resolved experiments such as transient Kerr-rotation [4–8] photoluminescence (PL) [9–11], reflection [12, 13] and absorption [14–16] spectroscopy were conducted to study the fundamental exciton dynamics, seeking to understand the valley polarization lifetime and the related valley pseudospin dynamics. In addition, the time-integrated degree of valley polarization was often studied by helicity-resolved PL measurements [1, 17, 18] and based on simple rate equations an estimation for the intervalley scattering time was obtained. However, the reported time scales for the exciton lifetime show a wide spreading in the reported values and the associated valley scattering mechanisms are still under intense debate. In this regard, a consistent understanding of the underlying processes has not been reached so far and a 'smoking gun experiment' that addresses and overcomes these discrepancies has yet to be demonstrated. In addition, most

of the previously reported measurements focus on either exfoliated or triangular shaped chemical vapor deposition (CVD) samples with smaller sizes of tens of microns. From the application point of view, the reliable production of huge amounts of larger size monolayer TMDCs [19, 20] are a key step for realizing future device fabrication of these 2D materials. However, large size TMDCs grown by CVD often suffer from large inhomogeneity concentrations and the associated defects may influence the optical excitation dynamics significantly. This may result in completely different valley exciton population decay and scattering mechanisms compared to more clean exfoliated monolayer samples. In this perspective, the precise and systematic characterization of the optical properties and the associated valley exciton dynamics in such large size monolayer TMDCs is pivotal to potential device applications in the future.

Here, we report on the valley exciton population and intervalley scattering dynamics in a large size CVD grown WSe_2 monolayer investigated by polarization controlled heterodyned transient grating (TG) spectroscopy. In TG spectroscopy two time-coincident non-collinear coherent pump laser pulses interfere at the sample surface and create a spatially modulated intensity or photon helicity pattern depending on their relative initial linear polarization states. Parallel polarization of the beams helps to study exciton diffusion and recombination, while cross polarization directly generates a spatial imbalance in the valley occupation and allows to directly probe the intervalley scattering dynamics. The simultaneous determination of exciton population and valley scattering dynamics applying a heterodyned and polarization-controlled detection scheme, provides the maximum information about the valley dynamics. Especially the polarization controlled TG method helps to precisely characterize the valley depolarization process and helps to distinguish it from the accompanied exciton population relaxation processes. Our findings reveal that in the large area CVD film sample, free exciton dynamics only dominate in the short time range of a few tens of picoseconds, accompanied by an extremely short intervalley scattering time of less than 1 ps. In contrast, the optical excitation relaxation dynamics in the long-time range are determined by the non-diffusive defect-bound excitons, whereby both population and valley scattering dynamics of the strapped excitons are substantially prolonged. Furthermore, temperature dependent dynamics indicate that the intervalley scattering of the trapped excitons strictly corresponds to the conservation of momentum, which requires the participation of two optical phonons at the *K/K'* point. The direct observation, and model-based identification as well as separation of the free and trapped exciton dynamics provide a so far rarely reported comprehensive understanding of valley exciton dynamics in CVD grown TMDC monolayers.

2. Experimental methods

The investigated WSe_2 monolayer (2D semiconductors, Inc., USA) was synthesized by low-pressure CVD. The sample was grown on a 1 cm × 1 cm *c*-cut sapphire substrate. Sample surface topography was characterized by atomic force microscopy (AFM) in non-contact mode (ParkNX10, ParkSystems).

The optical transitions around the band gap of the sample were measured with both steady state absorption at room temperature and PL spectroscopy at different temperatures ranging from 5 K to 300 K. The steady state PL and Raman spectra were measured using a micro-Raman setup equipped with a triple stage spectrometer (Spectroscopy and Imaging GmbH) and a liquid nitrogen cooled (150 K) CCD detector (PyLoN 100; Princeton Instruments).

In order to study the spatio-temporal dynamics of valley polarized excitons we make use of heterodyned, polarization controlled TG spectroscopy. This technique has been used previously to study quasiparticle dynamics [21, 22] and charge-density waves in superconductors [23], spin-helices and their propagation in quantum wells [24–26], fingerprints of fractional particles in quantum spin liquids [27], as well as exciton dynamics and exciton–exciton interactions in monolayer TMDCs [28–30].

In transient population grating spectroscopy (TPG), two coherent and parallel linearly polarized laser beams are overlapped on the sample surface. Interference of parallel polarized beams creates a periodic pattern of light intensity, which induces a spatially modulated excitation population pattern of photo-induced excitons with a spatial period Λ_{TPG} (figure 1(a)). Recording the grating decay dynamics for various spatial periods allows discrimination of recombination and diffusion relaxation mechanisms of the exciton population. For a simple excitation density independent diffusion process, the decay dynamics of the population grating $S_{TPG}(t)$ is a combined effect of the population relaxation and diffusion and can be written as

$$S_{TPG}(t) \propto \exp[-(D_X q^2 + \Gamma_X)t], \qquad (1)$$

where D_X is the diffusion coefficient of valley excitons, $q = 2\pi/\Lambda_{TPG}$ is the modulus of the grating wavevector and Γ_X is the relaxation rate of excitons including radiative and non-radiative recombination processes.

In contrast, overlapping two coherent cross-polarized beams leads to a spatially homogeneous intensity pattern and exciton population, while the electric field polarization is spatially modulated across the excitation spot and undergoes periodic changes between two opposite helicities [31]. Due to the optical selection rules in monolayer WSe_2, different helicities generate excitons in different valleys. In this way a spatially modulated valley density

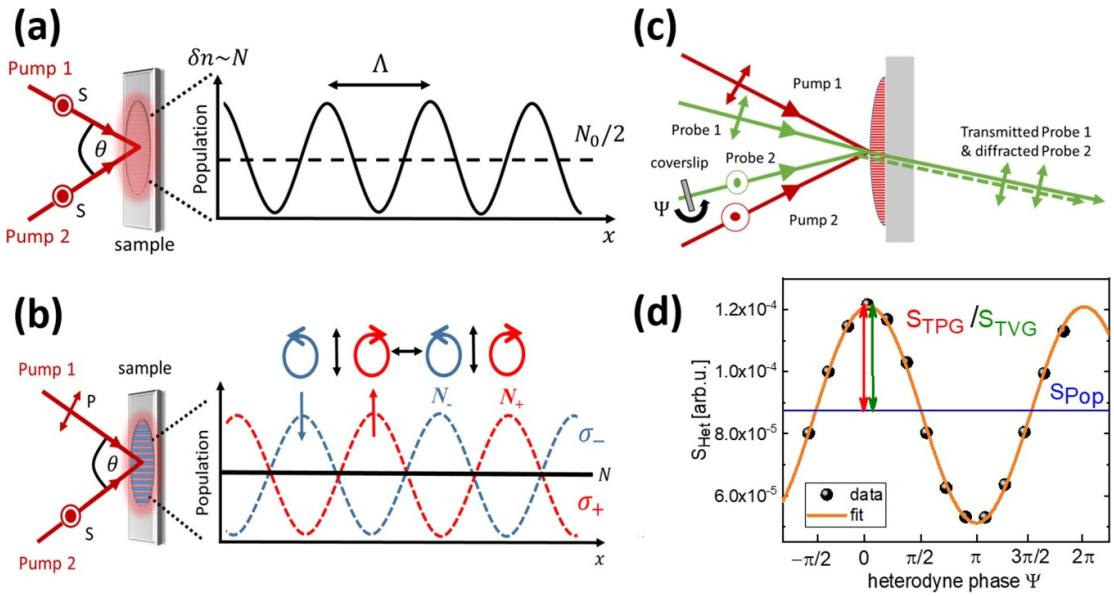

Figure 1. Principles of polarization selective heterodyned TG spectroscopy. (a) Illustration of the population grating with parallel polarized pump excitation beams. (b) Illustration of the spin or valley grating with cross polarized pump excitation beams. (c) Optical scheme for heterodyne detection of both population and grating signals. (d) Example of data collection with varying phase of the heterodyne beam at a fixed delay time, the mean value of the sinusoidal curve represents the population signal S_{POP}, while the amplitude of the sinusoidal modulation includes both population and grating signals $S_{TPG/TVG}$.

of wavelength Λ_{VG} is generated (figure 1(b)), which we refer to as the 'transient valley grating' (TVG) in accordance to [28]. Its decay encodes the valley depolarization, especially the intervalley scattering, as well as the spatial diffusion of the initially separated K and K' valley excitations. Hence, in analogy to the TPG, the TVG decay dynamics $S_{TVG}(t)$ can be expressed as

$$S_{TVG}(t) \propto \exp[-(D_X q^2 + \Gamma_X + \Gamma_{VS})t], \qquad (2)$$

where Γ_{VS} is the intervalley scattering rate. Note that, as for equation (1), this equation only holds if no multi-particle processes play a role in the grating dynamics. An interesting case where multiparticle processes do play a role has for instance been discussed in [30].

The present experiments use two phase related probe beams with linear polarizations to measure the temporal evolution of the grating decay via a heterodyne detection procedure (figure 1(c)). The probe beams are partially transmitted and partially diffracted by the excited sample, where the diffracted beam encodes the grating signal. The diffracted beam of the first probe is spatially overlapped with the transmitted beam from the second probe, which acts as a local oscillator to amplify the recorded signal. The heterodyne detected signal $S_{het}(\Psi)$ includes both population S_{POP} and grating $S_{TPG/TVG}$ signals, which can be expressed as

$$S_{het}(\Psi) = S_{POP} + S_{TPG/TVG} \cdot \cos(\Psi). \qquad (3)$$

Here, Ψ is the heterodyne phase which is controlled by a thin glass coverslip (figure 1(c)) that is put into one of the probe beams' optical path [32]. By controlling the time delay and relative phase of the two probe beams, the population and different kinds of grating signals can be detected simultaneously (figure 1(d)).

In all time-resolved experimental measurements, 200 fs pulsed laser beams were delivered from a MIRA 900F Ti:sapphire laser with a repetition rate of 76 MHz. Two different wavelengths (735 nm (≈1.69 eV) and 750 nm (≈1.65 eV)) were used to excite the sample. Using these excitation photon energies, different components of the excitonic states can be selectively excited due to blue shifting of the A-exciton resonance with varying temperatures (figure 2(b)). The four laser beams for the TG detection were arranged in the so-called BOXCAR geometry [32] and travelled through the same optical components. This special beam configuration ensures phase stability and self-alignment of the transmitted and diffracted probe beams and guarantees a fully controllable heterodyne probing procedure. More details on the experimental technique can be found in the supplementary material (available online at stacks.iop.org/2DM/8/035018/mmedia).

3. Results and discussion

Figure 2 shows the steady state spectroscopy characterization of the CVD monolayer WSe_2. The room temperature Raman spectrum (figure 2(a)) shows, consistent with the literature [33, 34], an optical phonon peak at around 250 cm^{-1}, which can be identified as the E' phonon mode, i.e. the in-plane relative motion of transition metal and chalcogen atoms.

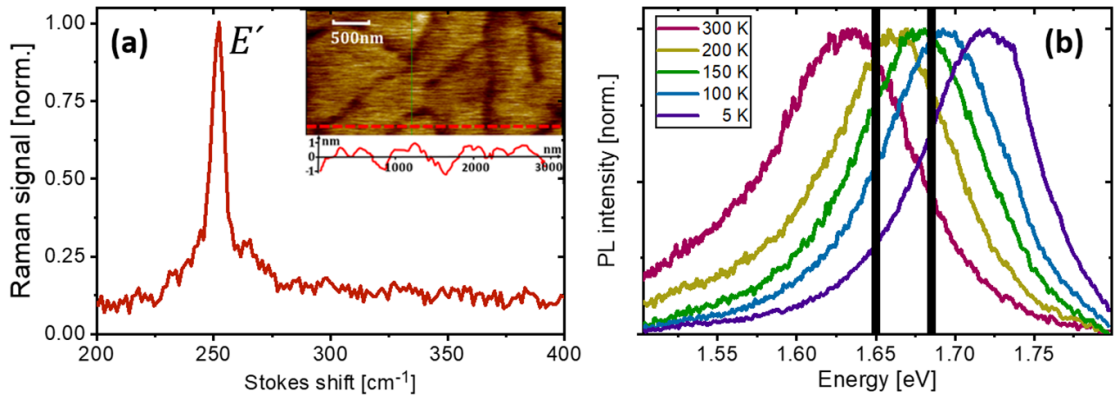

Figure 2. Characterization of the CVD grown film of monolayer WSe_2 on a *c*-cut sapphire substrate. (a) Raman spectrum at room temperature recorded with a continuous wave laser at 633 nm. Inset shows the AFM (atomic force microscopy) topography image and one scanning curve along the red dashed line in the image. (b) PL spectra at a few distinct temperatures obtained with femtosecond pulse laser at 670 nm and with weak energy of 1 pJ per pulse. The dashed lines indicate the two different excitation energies of 1.65 eV (750 nm) and 1.69 eV (735 nm) used for the TG measurements.

The weak intensity of the Raman scattering signal is probably caused by the presence of crystal inhomogeneities and large defects. The inset in figure 2(a) shows the AFM topography image of a typical part of the sample, and the corresponding height curve taken along the red dashed line in the image. The measured height variations are of the order of 1 nm, consistent with the variations reported for various TMDC monolayers [35–37]. The AFM results clearly show that the sample consists of randomly oriented domains with domain sizes of a few hundreds of nanometers and some discontinuities in the micron range. Figure 2(b) illustrates the PL spectra in vicinity of the A-exciton [36] energy measured at different temperatures. First, a large spectral peak shifting of about 100 meV was observed as temperature decreases from 300 K to 5 K. Second, the emission peaks at all temperatures are generally broad, with an overall width at half maximum of ∼100 meV and show only a slight narrowing for decreasing temperatures, in contrast to the few meV linewidth observed in homogeneous TMDC monolayers at cryogenic temperatures [38–40]. Apart from the large linewidth, the A-exciton PL emission also shows an asymmetrical shape originating from localized states located at lower energies extending deep inside the optical gap. A similar spectral shape and blue shift upon lowering the temperature has been observed in [41, 42], and is thought to be characteristic for p-type doped WSe_2 monolayer due to the presence of tungsten vacancy defects. In addition to this, also the large density of domain wall boundaries is expected to contribute to the density of trap states.

We furthermore note that the PL yield of the continuum film WSe_2 monolayer is extremely low ($\ll$1%). For a direct-gap semiconductor this means non-radiative recombination relaxation plays a dominant role. This again stands in stark contrast to the situation for exfoliated monolayers and is most likely due to the high defect density in CVD grown WSe_2. This is consistent with the large Stokes shift of ∼36 meV (figure S1 in supplementary material) which can be taken as a measure for the defect density [42]. This Stokes shift is an order of magnitude larger than that found for an exfoliated monolayer sample encapsulated in h-BN [42].

First, we focus on the temperature dependent exciton population dynamics. All experimental results were recorded under the same conditions with an excitation photon energy of 1.65 eV (750 nm) and an applied photon density of ∼4.2 μJ cm^{-2} (corresponding to an exciton density of about 4.8×10^{11} cm^{-2}, considering ∼3% absorption at 750 nm). As shown in figure 3, the population dynamics are complicated and follow a multi-exponential decay at all temperatures. To describe the whole population dynamics phenomenologically, we fit all the curves in figure 3

$$S_{\mathrm{POP}}(t) = \sum_{i=1}^{4} A_i \exp\left(-\frac{t}{\tau_i}\right), \qquad (4)$$

with A_i and τ_i being the amplitude and lifetime constant of each decay component. The obtained lifetimes are presented in table S1 in the supplementary material. In general, one can state that the whole population dynamics slow down as the temperature decreases. For example, at room temperature, the multi-exponential fitted lifetime constants are 2.6 ps, 17 ps, 149 ps and 1.75 ns, with relative amplitudes 47%, 23%, 17% and 13%, respectively, while at a moderately low temperature of 200 K, the lifetime constants change to 4.4 ps, 49 ps, 326 ps and 4.95 ns with relative amplitudes 9%, 27%, 23%, 41%, respectively.

The first two fast components can be assigned to the contribution stemming from the relatively free or shallow trapped excitons with lifetimes of

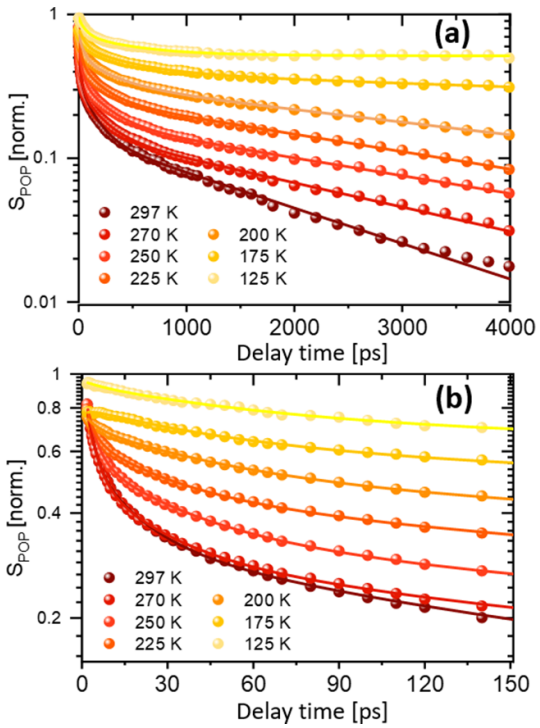

Figure 3. Exciton population dynamics of monolayer WSe_2 at different temperatures. Excitation is at 1.65 eV. Dots are experimental data and lines are multi-exponential fits. (a) Normalized dynamics on whole time range. (b) Normalized dynamics on short time range.

tens of picoseconds, while the last two components with longer lifetimes in the ns range likely display contributions from defect-bound and deep trapped excitons. These rough assignments are confirmed by the relative amplitudes of the two components. Considering the PL response (figure 2(b)) the laser excitation is at the high energy side of the A-exciton transition at room temperature exciting particularly free and defect-bound excitons. In contrast, at lower temperatures more and more defect-bound exciton states inside the gap are excited with naturally longer lifetimes. This process manifests itself in the temperature dependence of the amplitudes A_1 and A_4, as A_1 dominates at temperatures >220 K and strictly tends to zero for low temperatures. Oppositely, A_4 monotonically increases as the temperature decreases dominating the exciton population dynamics (see supplementary material). The second and third component also show a slowing down in their dynamics while having almost constant relative amplitudes at all temperatures. The slowing down of the global exciton population dynamics suggests a non-radiative dominated recombination process for all exciton species, which is in alignment with the obtained low PL quantum yield. Although a general understanding of the dynamics can be given in terms of free and defect-bound excitons, we note that a clear assignment of each of the four components is difficult, due to the inhomogeneity of the CVD sample, which is expected to lead to a variety of different traps (vacancies, defects, and domain boundaries).

We further point out that the observed multi-exponential decay dynamics cannot be understood in terms of exciton–exciton annihilation processes, since the excitation density dependent measurements show identical dynamics in the exciton density range $10^{11} - 10^{12}$ cm^{-2} (supplementary material). Interestingly, not only the dynamics, also the amplitude ratio between these components shows ignorable changes for increasing excitation density. This suggests that the defect density is larger than 10^{12} cm^{-2}, which manifests itself in the short lifetime and the very small diffusion length of the initial free excitons in the CVD sample, as we will point out later on when we discuss the TG measurements.

Now, we turn to the TG results for the CVD grown monolayer WSe_2, which are shown in figure 4. The associated decay dynamics were extracted from the heterodyne signals following the traditional method according to equations (1)–(3). In figures 4(a) and (b) the extracted dynamics for the exciton population, population grating, and valley grating signals are indicated as S_{POP}, S_{TPG}, and S_{TVG}, respectively. The 'pure' intervalley scattering dynamics, extracted by taking the ratio S_{TVG}/S_{TPG}, are shown in figures 4(c) and (d). Obviously, S_{POP} and S_{TPG}, obey identical dynamics at both temperatures as shown in figures 4(a) and (b), suggesting that diffusion processes play a negligible role to the observed long-time grating dynamics. First, the trapped exciton is non-diffusive. The observation that any free exciton diffusion effect is absent in the short time range is likely due to a small diffusion length of the free exciton compared to our grating period size. We note that previously in an exfoliated monolayer of WSe_2 with less inhomogeneities [29], the diffusion constant was estimated to be approximately 0.7 cm^2 s^{-1} (in the CVD sample one might expect it to be even smaller). Using this value as a rough estimate and considering the short lifetime of 10 ps gives a diffusion length of about 26 nm for the CVD grown monolayer sample. This value is orders of magnitude smaller than the grating period while being in the order of the domain sizes revealed by our AFM measurements. Hence, it is perfectly in line with the absence of diffusion revealed by the TPG measurements (see supplementary material).

In contrast to the population decay and grating dynamics S_{TPG}, the TVG signal S_{TVG} shows a much faster decay (green data points in figures 4(a) and (b)), indicating the existence of efficient intervalley scattering processes occurring on a time scale of hundreds of picoseconds (figures 4(c) and (d)), much longer than commonly reported values for other type of mechanically exfoliated TMDC monolayers [5, 43]. The valley scattering dynamics slow down as temperature decreases from 297 K to 150 K and the valley scattering dynamics obtained by considering

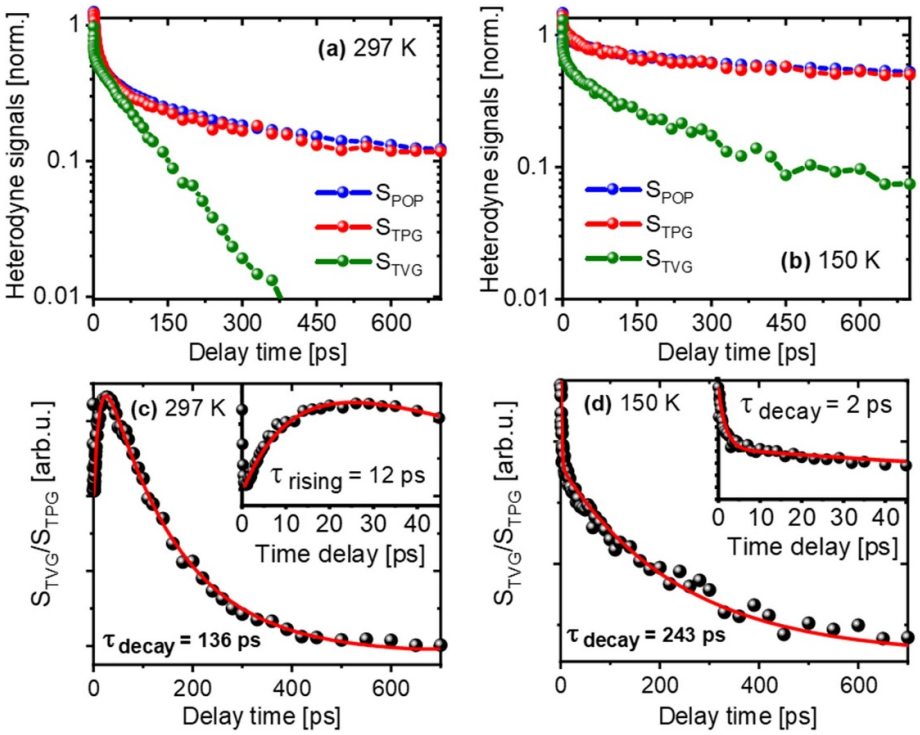

Figure 4. Panels (a) and (b) show the exciton population, S_{POP}, TPG, S_{TPG}, and the TVG, S_{TVG}, signals at 297 K and 150 K, respectively. Panels (c) and (d) display the extracted pure intervalley scattering dynamics at these temperatures. Open circles: data; red solid lines: bi-exponential fits. The inset shows the dynamics on the short time scales.

S_{TVG}/S_{TPG} (figures 4(c) and (d)) follows a single exponential decay with rate $\Gamma_{VS} = \tau_{VS}^{-1}$ only on the long-time scale (>50 ps).

In the short timescale (<50 ps), the valley grating shows a marked difference for both temperatures shown. While the dynamics shows a clear rising component at room temperature (see inset in figure 4(c)), this initial dynamic turns into a fast decay (∼2 ps) at 150 K.

Since by nature, an optically induced TG is expected to deteriorate with time, this intriguing initial growth dynamics seems to violate the intuition of a dynamic relaxation process and basic TG spectroscopic principle. A similar abnormal rising phenomenon in the population grating evolution has, however, been observed in a cuprate superconductor at low temperatures and high excitation densities [22]. There, the rising dynamics was interpreted in terms of an energy storing from the initial excited states to non-propagating modes forming a new index grating due to a two-particle recombination reaction. In contrast to the superconductor case, a similar mechanism causing such a phenomenon is non-existent in our experiments. Firstly, we did not observe such rising dynamics in the population grating transients, S_{TPG}, ruling out the possibility of exciting states with a higher grating diffraction efficiency after initial excitation. Secondly, the intervalley scattering process conserves energy, so that energy cannot be transferred to create a new grating pattern with an increased intervalley scattering efficiency.

Overall, considering the observed multi-exponential population dynamics and the spectral shift of the PL response with decreasing temperatures, we believe that the observed rising dynamics of the valley scattering has its origin in the mixing of different exciton species, i.e. excitons with not only different population (and diffusion) but also different valley scattering times. At room temperature, the excitation photon energy (1.65 eV) is located on the high energy side of the A-exciton transition where both free and trapped excitons can be excited. In contrast, at 150 K the excitation is on the low energy side of the excitonic transition where the dominating excitation are trapped exciton species. This idea is further substantiated by the more detailed temperature dependence and the response at different excitation photon energies. As presented in figure 5(a) (excitation energy at 1.65 eV), the extracted rising component continually fades off as temperature decreases until it fully disappears at around 200 K, where the excitation energy becomes lower than the peak absorption (see figure 2(b)). Switching the excitation photon energy to 1.69 eV at 200 K, thereby again exciting in the high energy part of the excitonic absorption, brings back the rising component (see figure 5(b)). For this excitation energy one has to go to 125 K to suppress the rising response, again consistent with the fact that at this temperature the lower part of the excitonic absorption is excited for this energy (see figure 2(b)).

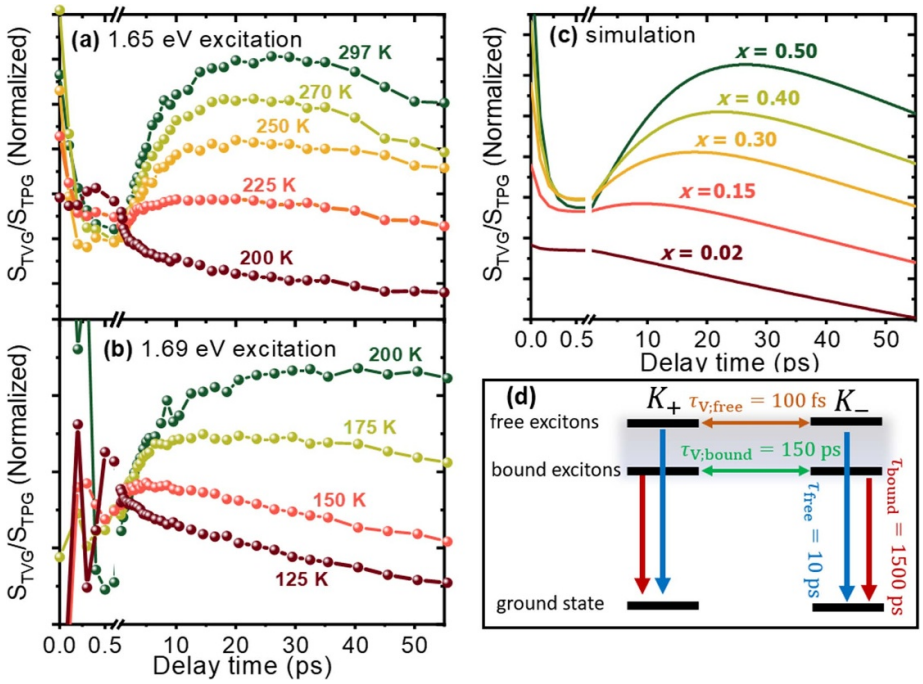

Figure 5. Temperature dependence of pure valley scattering dynamics in the short time range and two-state model simulations. (a) Excitation at 1.65 eV. (b) Excitation at 1.69 eV. (c) Simulated dynamics. (d) Two-state kinetic model of exciton population and valley scattering dynamics.

Based on these observations, we simulated the extracted dynamics with a simple phenomenological kinetic model to give a clearer and intuitive understanding. We still follow the traditional analysis by considering the ratio S_{TVG}/S_{TPG}, while modeling both population grating S_{TPG} and the valley grating dynamics S_{TVG} as a double-exponential decay process originating from contributions of the free and trapped excitons respectively (for details see supplementary material). For simplicity, we only focus on the intervalley scattering grating processes. Hence, the diffusion of the unbound excitons is captured by a composite lifetime τ_{TPG} of the grating dynamics, whereas for the trapped excitons we identify $\tau_{TPG} = \tau_{POP}$, i.e. we assume the absence of diffusion, consistent with the data. The model is schematically depicted in figure 5(d), where the first process (orange double arrow) represents the contribution from the free excitons, with a short exciton population grating lifetime and intervalley scattering lifetime of ∼10 ps (blue arrow) and ∼100 fs (green double arrow), respectively. The second process represents the contribution from the trapped excitons, with a long exciton population and intervalley scattering lifetime of ∼1500 ps (red arrow) and ∼150 ps (green double arrow), respectively. The order of magnitude of the considered recombination lifetimes for the free and defect bound excitons stem from the obtained exciton population dynamics presented in figure 3. For simplicity, all the time constants are considered temperature independent. The proportion of the amplitude of these two processes is set to x and $(1 - x)$ and does vary with temperature due to the temperature dependence of the excitonic energy (figure 2(b)). Figure 5(c) shows that a simulation using this simple model captures the measured dynamics quiet well, supporting the existence of different exciton species upon optical excitation of the CVD sample.

Having understood the puzzle in the short time range of the intervalley scattering dynamics, we now focus on the long-time range >50 ps where the intervalley scattering dynamics is dominated by the trapped excitons only and can be approximately accounted for by a single exponential decay. As indicated in figure 6(a), the measured intervalley scattering dynamics slows down as temperature decreases. This slowing down of the dynamics can be understood in terms of two aspects. The major one is the interaction of excitons with the crystal lattice, i.e. at low temperature the phonon population decreases massively following the Bose–Einstein distribution and thus reduces the amount of total exciton-phonon scattering interactions. The minor one could come from the proportion of different trapped exciton species, i.e. as temperature decreases deeper trapped excitonic states are excited, due to the blue shifting of the optical response, which may be expected to have longer intervalley scattering lifetimes. The latter was indeed confirmed by measurements at fixed temperatures using different excitation photon energies. As an example, at 150 K, the intervalley scattering dynamics upon excitation at 1.65 eV indeed slows down compared to that at 1.69 eV (figure S5(b) in supplementary material). This, however, is only a minor effect showing that the

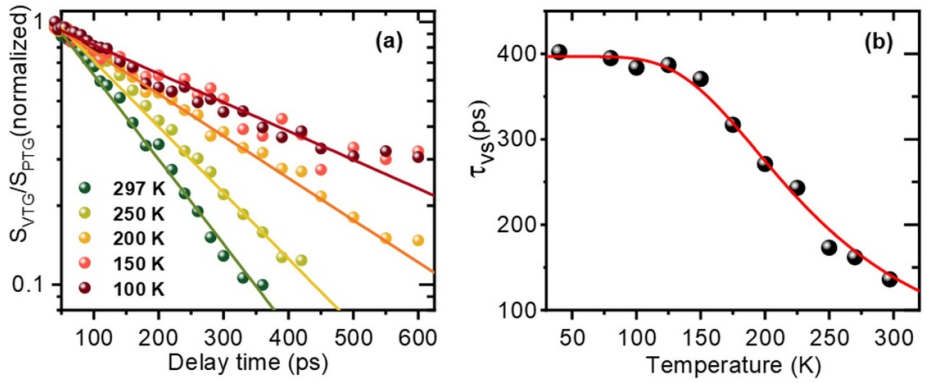

Figure 6. Temperature dependent valley scattering dynamics in the long-time range using 1.65 eV excitation energy. (a) Temperature dependence of the normalized dynamics (symbols) and single exponential fits (straight lines) plotted on a logarithmic scale. (b) Extracted scattering times at different temperatures. The solid lines correspond to the phonon contribution.

exciton-phonon scattering processes dominate the temperature dependence. In order to relate these considerations to our data mainly focusing on the general behavior, we ignore minor differences in lifetimes of different deep trapped excitons, and a temperature dependent exciton intervalley scattering rate was fitted to the data (figure 6(b), symbols):

$$\tau_{VS}{}^{-1} = A + C[\exp\ (\hbar\Omega/k_B T) - 1]^{-1}, \qquad (5)$$

where A represents the temperature independent rate, C can be interpreted as a measure for the exciton-phonon coupling strength, and Ω is the phonon frequency. Clearly, figure 6(b) (solid line) shows a very satisfactory accordance of equation (5) with the data. Very interestingly, we find $\hbar\Omega = (69 \pm 7)$ meV for the phonon energy, which is comparable to the two-optical phonon energy ~ 64 meVat the momentum space K (K') point for monolayer WSe_2 [44, 45]. Although exciton scattering from K (K') valley to K' (K) valley does not change the exciton energy and conserves the total centre of mass momentum, a simultaneous transfer of both the electron's and hole's momentum by ± 2 K between them is indeed a necessary process. We thus speculate that the intervalley scattering of the trapped excitons in monolayer WSe_2 incorporates the emission and absorption of two optical phonons.

Comparing to the dynamics of the free excitons, the most intriguing question is why the intervalley scattering lifetime of the trapped excitons is prolonged by more than three orders. Similar long exciton valley scattering times have been observed in triangular-shaped monolayer WSe_2, where the associated dynamics [46] was interpreted as originating from the pseudo-spin transfer from photo-carriers to the holes in the ground state, which results in an exciton valley scattering lifetime much longer than the population lifetime. Our result cannot be understood within this picture, since the observed trapped exciton population lifetime here is still much longer than the valley scattering lifetime (figure 4). Recently, experiments on an electron beam bombarded WSe_2 monolayer [47] demonstrated that excitons trapped by Se-vacancy defects change the valley scattering lifetime, extending up to even microseconds at low temperature of 10 K. There, this astonishing observation was discussed in terms of a theoretical calculation [48] in which excitonic optical transitions between the defect states and the pristine crystal quasiparticle state inherit the circular dichroism selectivity. It was further assumed that intervalley scattering processes for the formed trapped exciton states are negligible. In addition, we note that except from the lower exciton transition energy, this electron beam bombarded, n-type sample has an inhomogeneous PL linewidth and asymmetric line shape which is similar to the PL from our p-type doped CVD sample. Possibly, both kinds of defect trapped excitons share a common reason for the long-lived valley scattering time. It is well-known that for the occurrence of the intervalley scattering, there are two prerequisites: conservation of momentum and a simultaneous spin flip of both of electron and hole inside the forming exciton. The former requires interaction with phonons, in line with the temperature dependence of the scattering lifetime discussed above. In addition, the charged W-vacancy defects are expected to locally increase the screening of the Coulomb exchange interaction within the trapped exciton, and hence making the often-considered electron–hole exchange [49, 50] spin flip process less efficient, thereby allowing for a longer-lived valley polarization.

4. Conclusion

In conclusion, we have investigated both the exciton population and the valley pseudospin dynamics in a large size CVD grown WSe_2 continuum monolayer applying polarization controlled TG spectroscopy. Using this spectroscopic technique, a local imbalance of the valley polarized excitons was induced in real space that probes the intervalley scattering

dynamics directly. Based on the above discussion, the TVG measurements revealed that the dynamics of the population and valley scattering are dominated by the sample inhomogeneity and the associated defect-induced states. Our data suggests that the localized excitons are more robust to intervalley scattering, although the detailed understanding of the intervalley scattering mechanisms of defect trapped excitons is still an open question. The intervalley scattering dynamics show two distinct time regimes. We identified a short-lived exciton state with extremely short valley scattering times of hundreds of fs, which most likely is due to the electron–hole exchange interaction of free excitons as discussed earlier in literature [49, 50]. In contrast to the free exciton, defect trapping can substantially increase both the population and the valley scattering lifetimes. Mixing of free and defect-bound exciton response dominates the first 50 ps of the TVG dynamics, causing an anomalous increase. This phenomenon can be understood in terms of a simple kinetic model based on the presence of free and defect bound excitons. Our findings indicate that the degree of disorder in the 2D monolayer limit might be an important tuning knob in order to control the intervalley scattering time thus providing an interesting route towards realization of TMDC based valleytronic devices. We speculate that defect engineering and the precise control of disorder may help tailoring robust valley pseudospin properties in monolayer TMDCs.

Data availability statement

The data that support the findings of this study are available upon reasonable request from the authors.

Acknowledgments

The authors acknowledge financial support funded by the Deutsche Forschungsgemeinschaft (DFG) through the Project No. 277146847-CRC1238, Control and Dynamics of Quantum Materials (Subproject No. B05).

ORCID iDs

Julian Wagner https://orcid.org/0000-0001-8325-9373
Jingyi Zhu https://orcid.org/0000-0003-0519-4724
Paul H M van Loosdrecht https://orcid.org/0000-0002-3704-9890

References

[1] Zeng H, Dai J, Yao W, Xiao D and Cui X 2012 Valley polarization in MoS_2 monolayers by optical pumping *Nat. Nanotechnol.* **7** 490–3
[2] Ye Z, Sun D and Heinz T F 2017 Optical manipulation of valley pseudospin *Nat. Phys.* **13** 26–9
[3] Schaibley J R, Yu H, Clark G, Rivera P, Ross J S, Seyler K L, Yao W and Xu X 2016 Valleytronics in 2D materials *Nat. Rev. Mater.* **1** 16055
[4] LaMountain T, Bergeron H, Balla I, Stanev T K, Hersam M C and Stern N P 2018 Valley-selective optical Stark effect probed by Kerr rotation *Phys. Rev.* B **97** 045307
[5] Plechinger G, Korn T and Lupton J M 2017 Valley-polarized exciton dynamics in exfoliated monolayer WSe_2 *J. Phys. Chem.* C **121** 6409–13
[6] Yan T, Ye J, Qiao X, Tan P and Zhang X 2017 Exciton valley dynamics in monolayer WSe_2 probed by the two-color ultrafast Kerr rotation *Phys. Chem. Chem. Phys.* **19** 3176–81
[7] Yang L, Sinitsyn N A, Chen W, Yuan J, Zhang J, Lou J and Crooker Scot A 2015 Long-lived nanosecond spin relaxation and spin coherence of electrons in monolayer MoS_2 and WS_2 *Nat. Phys.* **11** 830–4
[8] Plechinger G, Nagler P, Arora A, Schmidt R, Chernikov A, Del Águila A G, Christianen P C M, Bratschitsch R, Schüller C and Korn T 2016 Trion fine structure and coupled spin-valley dynamics in monolayer tungsten disulfide *Nat. Commun.* **7** 12715
[9] Wang G, Palleau E, Amand T, Tongay S, Marie X and Urbaszek B 2015 Polarization and time-resolved photoluminescence spectroscopy of excitons in $MoSe_2$ monolayers *Appl. Phys. Lett.* **106** 112101
[10] Yan T, Qiao X, Liu X, Tan P and Zhang X 2014 Photoluminescence properties and exciton dynamics in monolayer WSe_2 *Appl. Phys. Lett.* **105** 101901
[11] You Y, Zhang -X-X, Berkelbach T C, Hybertsen M S, Reichman D R and Heinz T F 2015 Observation of biexcitons in monolayer WSe_2 *Nat. Phys.* **11** 477–81
[12] Ceballos F, Cui Q, Bellus M Z and Zhao H 2016 Exciton formation in monolayer transition metal dichalcogenides *Nanoscale* **8** 11681–8
[13] Shin M J, Kim D H and Lim D 2014 Photoluminescence saturation and exciton decay dynamics in transition metal dichalcogenide monolayers *J. Korean Phys. Soc.* **65** 2077–81
[14] Cui Q, He J, Bellus M Z, Mirzokarimov M, Hofmann T, Chiu H-Y, Antonik M, He D, Wang Y and Zhao H 2015 Transient absorption measurements on anisotropic monolayer ReS_2 *Small* **11** 5565–71
[15] Kumar N, He J, He D, Wang Y and Zhao H 2013 Charge carrier dynamics in bulk MoS_2 crystal studied by transient absorption microscopy *J. Appl. Phys.* **113** 133702
[16] Cui Q, Ceballos F, Kumar N and Zhao H 2014 Transient absorption microscopy of monolayer and bulk WSe_2 *ACS Nano* **8** 2970–6
[17] Mak K F, He K, Shan J and Heinz T F 2012 Control of valley polarization in monolayer MoS_2 by optical helicity *Nat. Nanotechnol.* **7** 494–8
[18] Wang G, Bouet L, Lagarde D, Vidal M, Balocchi A, Amand T, Marie X and Urbaszek B 2014 Valley dynamics probed through charged and neutral exciton emission in monolayer WSe_2 *Phys. Rev.* B **90** 075413
[19] Dong R and Kuljanishvili I 2017 Review article: progress in fabrication of transition metal dichalcogenides heterostructure systems *J. Vac. Sci. Technol.* B **35** 030803
[20] Shi Y, Li H and Li L-J 2015 Recent advances in controlled synthesis of two-dimensional transition metal dichalcogenides via vapour deposition techniques *Chem. Soc. Rev.* **44** 2744–56
[21] Gedik N, Orenstein J, Liang R, Bonn D A and Hardy W 2004 Non-equilibrium quasiparticle dynamics in single crystals of YBCO ortho II *Physica* C **408–410** 690–1
[22] Gedik N, Orenstein J, Liang R, Bonn D A and Hardy W N 2003 Diffusion of nonequilibrium quasi-particles in a cuprate superconductor *Science* **300** 1410–2
[23] Torchinsky D H, Mahmood F, Bollinger A T, Božović I and Gedik N 2013 Fluctuating charge-density waves in a cuprate superconductor *Nat. Mater.* **12** 387–91

[24] Yang L, Koralek J D, Orenstein J, Tibbetts D R, Reno J L and Lilly M P 2012 Coherent propagation of spin helices in a quantum-well confined electron gas *Phys. Rev. Lett.* **109** 246603
[25] Koralek J D, Weber C P, Orenstein J, Bernevig B A, Zhang S-C, Mack S and Awschalom D D 2009 Emergence of the persistent spin helix in semiconductor quantum wells *Nature* **458** 610–3
[26] Cameron A R, Riblet P and Miller A 1996 Spin gratings and the measurement of electron drift mobility in multiple quantum well semiconductors *Phys. Rev. Lett.* **76** 4793–6
[27] Zhang H, Kim S, Kim Y-J, Kee H-Y and Yang L 2019 (arXiv:1908.04807)
[28] Mahmood F, Alpichshev Z, Lee Y-H, Kong J and Gedik N 2018 Observation of exciton–exciton interaction mediated valley depolarization in monolayer $MoSe_2$ *Nano Lett.* **18** 223–8
[29] Wang J, Guo Y, Huang Y, Luo H, Zhou X, Gu C and Liu B 2019 Diffusion dynamics of valley excitons by transient grating spectroscopy in monolayer WSe_2 *Appl. Phys. Lett.* **115** 131902
[30] Kuhn H, Wagner J, Han S, Bernhardt R, Gao Y, Xiao L, Zhu J and Van P H M 2020 Excitonic transport and intervalley scattering dynamics in large-size exfoliated $MoSe_2$ monolayer investigated by heterodyned transient grating spectroscopy *Laser Photonics Rev.* **14** 2000029
[31] Fourkas J T, Trebino R and Fayer M D 1992 The grating decomposition method: a new approach for understanding polarization-selective transient grating experiments. I. Theory *J. Chem. Phys.* **97** 69–77
[32] Gedik N and Orenstein J 2004 Absolute phase measurement in heterodyne detection of transient gratings *Opt. Lett.* **29** 2109–11
[33] Chen S Y, Zheng C X, Fuhrer M S and Yan J 2015 Helicity-resolved Raman scattering of MoS_2, $MoSe_2$, WS_2, and WSe_2 atomic layers *Nano Lett.* **15** 2526–32
[34] De Luca M, Cartoixà X, Martin-Sánchez J, López-Suárez M, Trotta R, Rurali R and Zardo I 2020 New insights in the lattice dynamics of monolayers, bilayers, and trilayers of WSe_2 and unambiguous determination of few-layer-flakes' thickness *2D Mater.* **7** 025004
[35] Liu B, Fathi M, Chen L, Abbas A, Ma Y and Zhou C 2015 Chemical vapor deposition growth of monolayer WSe_2 with tunable device characteristics and growth mechanism study *ACS Nano* **9** 6119–27
[36] Gutiérrez H R, Perea-López N, Elías A L, Berkdemir A, Wang B, Lv R, López-Urías F, Crespi V H, Terrones H and Terrones M 2013 Extraordinary room-temperature photoluminescence in triangular WS_2 monolayers *Nano Lett.* **13** 3447–54
[37] Han S, Boguschewski C, Gao Y, Xiao L, Zhu J and Van Loosdrecht P H M 2019 Incoherent phonon population and exciton–exciton annihilation dynamics in monolayer WS_2 revealed by time-resolved resonance Raman scattering *Opt. Express* **27** 29949–61
[38] Moody G *et al* 2015 Intrinsic homogeneous linewidth and broadening mechanisms of excitons in monolayer transition metal dichalcogenides *Nat. Commun.* **6** 8315
[39] Jakubczyk T, Delmonte V, Koperski M, Nogajewski K, Faugeras C, Langbein W, Potemski M and Kasprzak J 2016 Radiatively limited dephasing and exciton dynamics in $MoSe_2$ monolayers revealed with four-wave mixing microscopy *Nano Lett.* **16** 5333–9
[40] Scarpelli L, Masia F, Alexeev E M, Withers F, Tartakovskii A I, Novoselov K S and Langbein W 2017 Resonantly excited exciton dynamics in two-dimensional $MoSe_2$ monolayers *Phys. Rev.* B **96** 045407
[41] Zhang S, Wang C-G, Li M-Y, Huang D, Li L-J, Ji W and Wu S 2017 Defect structure of localized excitons in a WSe_2 monolayer *Phys. Rev. Lett.* **119** 046101
[42] Tran K, Singh A, Seifert J, Wang Y, Hao K, Huang J-K, Li L-J, Taniguchi T, Watanabe K and Li X 2017 Disorder-dependent valley properties in monolayer WSe_2 *Phys. Rev.* B **96** 041302
[43] Ye J, Niu B, Li Y, Li T and Zhang X 2017 Exciton valley dynamics in monolayer $Mo_{1-x}W_xSe_2$ ($x = 0, 0.5, 1$) *Appl. Phys. Lett.* **111** 152106
[44] Sahin H, Tongay S, Horzum S, Fan W, Zhou J, Li J, Wu J and Peeters F M 2013 Anomalous Raman spectra and thickness-dependent electronic properties of WSe_2 *Phys. Rev.* B **87** 165409
[45] Sengupta A, Chanana A and Mahapatra S 2015 Erratum: 'Phonon scattering limited performance of monolayer MoS_2 and WSe_2 n-MOSFET' *AIP Adv.* **5** 029901
[46] Hsu W-T, Chen Y-L, Chen C-H, Liu P-S, Hou T-H, Li L-J and Chang W-H 2015 Optically initialized robust valley-polarized holes in monolayer WSe_2 *Nat. Commun.* **6** 8963
[47] Moody G, Tran K, Lu X, Autry T, Fraser J M, Mirin R P, Yang L, Li X and Silverman K L 2018 Microsecond valley lifetime of defect-bound excitons in monolayer WSe_2 *Phys. Rev. Lett.* **121** 057403
[48] Refaely-Abramson S, Qiu D Y, Louie S G and Neaton J B 2018 Defect-induced modification of low-lying excitons and valley selectivity in monolayer transition metal dichalcogenides *Phys. Rev. Lett.* **121** 167402
[49] Maialle M Z, de Andrada e Silva E A and Sham L J 1993 Exciton spin dynamics in quantum wells *Phys. Rev.* B **47** 15776–88
[50] Yu T and Wu M W 2014 Valley depolarization due to intervalley and intravalley electron–hole exchange interactions in monolayer MoS_2 *Phys. Rev.* B **89** 205303